Magnetic order in superconducting $TbMo_6S_8$, $DyMo_6S_8$, and $ErMo_6S_8$

W. Thomlinson and G. Shirane
Brookhaven National Laboratory, Upton, New York 11973

D. E. Moncton
Bell Laboratories, Murray Hill, New Jersey 07974

M. Ishikawa and Ø. Fischer
Departément de Physique de la Matière Condensée, Université de Genève, 1211 Genève 4, Switzerland

(Received 23 September 1980)

$DyMo_6S_8$ and $TbMo_6S_8$ are superconducting below $T_c = 2.05$ K, and $ErMo_6S_8$ below $T_c = 2.2$ K. Neutron diffraction has been used to study the development of magnetic order in these materials at temperatures T_M less than T_c. In zero applied magnetic field, the $DyMo_6S_8$ and $TbMo_6S_8$ order antiferromagnetically, the magnetic order coexisting with the superconductivity. The $ErMo_6S_8$ sample showed no long-range magnetic order when initially cooled down in zero applied magnetic field. After a magnetic field was applied and reduced to near zero, the sample showed coexistent antiferromagnetic order below $T_M = 0.2$ K. Magnetization measurements on $DyMo_6S_8$ and $TbMo_6S_8$ at temperatures below T_M suggest the development of ferromagnetic order as the applied field increases. In the case of $TbMo_6S_8$, the neutron data show ferromagnetic order developing for $H \geq H_{c2}$ where H_{c2} is the upper critical field for superconductivity. For $DyMo_6S_8$ ferromagnetic order develops for H much less than H_{c2}. Both ferromagnetic and antiferromagnetic order occur with the sample in the superconducting state.

I. INTRODUCTION

A significant amount of theoretical and experimental effort has been expended over the past few years in an attempt to understand the interaction of magnetic order with superconductivity. The basic question has been whether or not long-range magnetic order can coexist with superconductivity, and, if so, what modifications of the various states occur. Of particular interest has been the form of the magnetic structures possible, and the interactions between the two competing states.

Until a few years ago, most of the effort involved the substitution of magnetic ions into superconductors to study the effects of the superconducting state.[1] The results have been understood on the basis of the Abrikosov-Gorkov spin-depairing mechanism.[2] The superconductivity was generally suppressed before the concentration of magnetic ions became sufficiently high for long-range magnetic order to occur.

The problems associated with the substitutional alloys have been overcome with the synthesis of superconducting stoichiometric rare-earth compounds in which the magnetic rare-earth ions are distributed over regular lattice sites.[3–5] These new compounds have provided the opportunity of studying the interaction of superconductivity with long-range magnetic order. The discovery of anomalies in the electrical, magnetic, and thermal properties of these superconductors suggested the development of ordered magnetic states.[6–9] The development of magnetic order in two such materials, $ErRh_4B_4$ (Ref. 6) and $HoMo_6S_8$ (Ref. 7), at temperatures below the superconducting transition temperature T_c ultimately destroys the superconducting state at a second transition at T_{c2}. Neutron scattering studies of these reentrant transitions have confirmed the ferromagnetic ordering of the rare-earth ions in both materials.[10,11] Recent neutron scattering and heat-capacity experiments on $ErRh_4B_4$ and $HoMo_6S_8$ have investigated the competition between the magnetic order and the superconductivity. In a narrow temperature range above T_{c2}, coexistence of superconductivity with an oscillatory ($\lambda > 100$ Å) magnetization has been observed in both $HoMo_6S_8$ (Ref. 12) and $ErRh_4B_4$ (Refs. 13 and 14). Although the small-angle scattering produced by this magnetization is essentially resolution limited in both compounds, intensity measurements suggest that the ordering in $HoMo_8S_8$ is more likely to be long ranged than it is in $ErRh_4B_4$.

Other members of the Chevrel phase class of materials, $(R)Mo_6X_8$ where R = rare earth and X = S or Se, become magnetically ordered at temperatures below the superconducting transition temperature T_c without destroying the superconducting state. Several review articles have discussed these results and the reader is referred to the references.[13,15,16]

Evidence of coexistence in $(R)Mo_6S_8$ (R = Tb, Dy, and Er) was reported by Ishikawa and Fischer.[9]

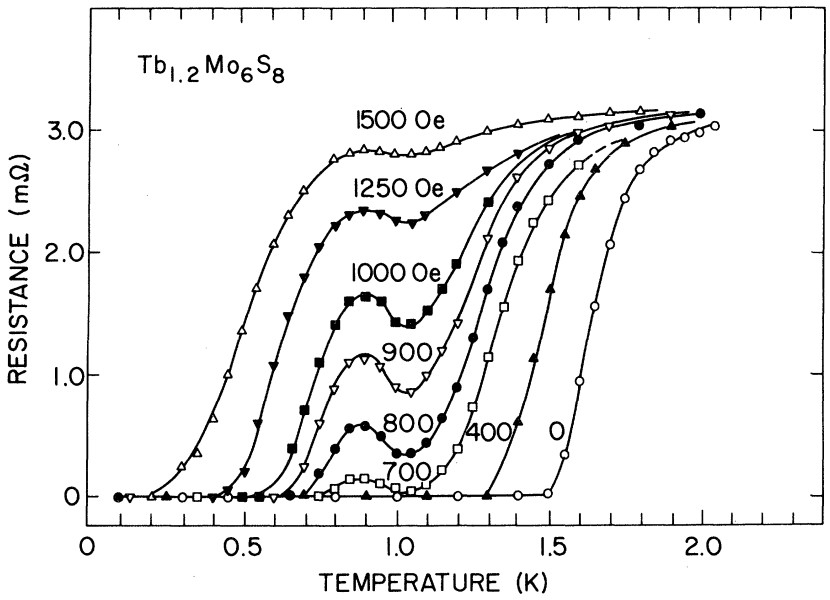

FIG. 1. Resistance vs temperature for $TbMo_6S_8$ in magnetic fields between 0 and 1.5 kOe. After Ishikawa and Fischer, Ref. 9.

Resistance anomalies were found in the superconducting state and were interpreted as being the result of magnetic ordering by means of ac susceptibility and magnetization measurements.[17] The coexistence of the antiferromagnetic order of the R ions in the Chevrel phase with the superconducting state has been confirmed by neutron scattering experiments on $DyMo_6S_8$,[18] $TbMo_6S_8$,[19] and $GdMo_6S_8$.[20] The neutron scattering experiments, by themselves, cannot prove coexistence since they are not sensitive to the superconducting state. However, by carrying out the neutron experiments on the identical samples used for the resistivity, susceptibility, and upper critical-field experiments, the proper correlation of the sample properties has been made.

Ishikawa and Fischer[9] have reported anomalies in the upper critical fields, H_{c2}, of several coexistent materials, and the neutron scattering experiments have confirmed that the anomalies are associated with the magnetic transitions.[18,19] Also, the resistivity curves for these materials are affected by the presence of small applied external magnetic fields. For small applied fields, $H < H_{c2}$, the magnetic transition is accompanied by the development of finite resitivity. Figure 1, as an example, shows the resistivity curves for $TbMo_6S_8$ as a function of magnetic field. The peak in resistivity corresponds to the temperature range where the magnetic order is developing.

The magnetization data of Ishikawa and Muller,[17] shown in Fig. 2, also show interesting behavior. Above T_M, the magnetization curves for $DyMo_6S_8$ and $TbMo_6S_8$ are those associated with a paramagnet. Below T_M, the curve for $TbMo_6S_8$ shows a transition from antiferromagnetic behavior to ferromagnetic at $H \sim H_{c2} = 1.9$ kOe. Above H_{c2}, the field is sufficient to flip the staggered spins and ferromagnetic order develops along the direction of the applied field. However, for $DyMo_6S_8$, the magnetization curve behaves like a ferromagnet for fields as low as 200 Oe, much below $H_{c2} \sim 1.2$ kOe. Ishikawa and Muller suggest that between 200 Oe and 1.2 kOe, the sample is an induced ferromagnetic superconductor.

These effects of applied magnetic fields suggested the importance of studying $DyMo_6S_8$ and $TbMo_6S_8$ by neutron diffraction in applied fields. The results of the magnetic field work will be discussed in this paper. In addition, the neutron scattering experiments on the coexistence problem in $ErMo_6S_8$ will be presented, since they were also done in a magnetic field.

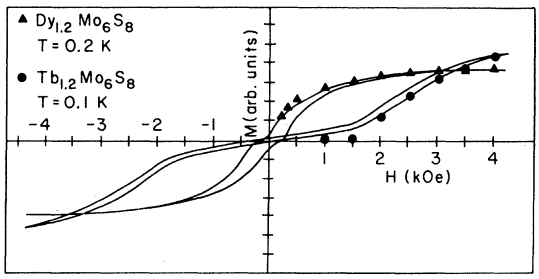

FIG. 2. Magnetization as a function of applied magnetic field for $TbMo_6S_8$ and $DyMo_6S_8$ calculated from the {100} peak intensity. The solid curves are the magnetization data of Ishikawa and Muller, Ref. 17. The neutron data are normalized to the magnetization data at 4 kOe.

II. EXPERIMENTAL DETAILS

The neutron scattering experiments were carried out at the Brookhaven National Laboratory high-flux-beam reactor using triple-axis spectrometers set for elastic scattering. The incident beam had a constant energy of 13 meV provided by a pyrolytic graphite monochromator. A pyrolytic graphite filter was placed before the sample to suppress higher-order wavelengths. The samples were mounted in a helium dilution refrigerator which could be inserted into a superconducting magnet capable of generating fields up to 70 kOe. The physical shapes of the three samples were different: the $DyMo_6S_8$ was a sintered cylinder, the $TbMo_6S_8$ was a finely ground powder, and the $ErMo_6S_8$, also a finely ground powder, was mixed with an equal volume of Al powder and pressed into a cylinder. Good thermal contact of all samples with the thermometry and refrigerator was observed at all temperatures.

As noted above, the samples used in the neutron scattering experiments were all very well characterized by resistivity, susceptibility, and magnetization experiments. With the exception of the $ErMo_6S_8$ sample, they were the same samples reported in the literature.[9,17] The $ErMo_6S_8$ sample was independently checked for its superconducting properties and found to be the same as the one described in Ref. 17.

The proportions of the starting materials in the preparation of these samples give nominal compositions of $(R)_{1.2}Mo_6S_8$. However, the neutron-diffraction intensities are consistent with the stoichiometric composition of the Chevrel phase. The distribution of the extra rare-earth material in the samples is not known. In general, we have not been able to identify second phases, although small magnetic-impurity peaks indicate their presence. For these reasons, we have referred to the materials by their stoichiometric compositions throughout the text.

III. RESULTS AND DISCUSSION

A. Zero applied magnetic field

In this section, the neutron scattering results in zero applied magnetic field for the $TbMo_6S_8$ and $DyMo_6S_8$ are presented. Since the data for $DyMo_6S_8$ have been published in detail,[18] we will concentrate on the $TbMo_6S_8$, in particular those aspects of the data not covered sufficiently in an earlier publication.[19]

The $TbMo_6S_8$ powder diffraction pattern at $T=4.2$ K is shown in Fig. 3. The nuclear peak intensities have ratios which are in agreement with those calculated using the positional parameters of Yvon.[21] When the sample is cooled to $T=0.07$ K, it is seen that a series of superlattice peaks develops. These peaks have been indexed with half-integer values, corresponding to a simple antiferromagnetic structure consisting of (001) planes with the spin direction alternating between planes. In order to establish that the magnetic order is long range, the width of the $\{00\frac{1}{2}\}$ peak was compared with the instrumental resolution and found to be resolution limited. This allows us to set a lower limit of ~ 300 Å on the correlation length.

The magnitude of the magnetic moment can be calculated by comparison of the measured magnetic-peak intensities with the calculated intensities. An absolute calibration is provided by normalization of the scattering intensities with the nuclear-peak intensities. For this calculation, the crystal can be taken as having a tetragonal magnetic structure, neglecting the slight trigonal distortion. Each peak group is then integrated to determine the intensity, neglecting any small splitting of the peaks. The angle, ϕ, between the wave vector of the magnetization, $\vec{q}_m=(0,0,\frac{1}{2})$ and the magnetic moment axis is allowed to vary. At each angle, the ratios of the magnetic peaks relative to the $\{00\frac{1}{2}\}$ peak are calculated. The best fit with the experimental data gave $\phi\sim 60°$ for $TbMo_6S_8$, $\phi\sim 55°$ for $DyMo_6S_8$, and $\phi\sim 45°$ for $ErMo_6S_8$ with an uncertainty of $\pm 5°$ on the angle.

The magnetic moment can be calculated using this angle of ϕ and the spherical magnetic form factor calculated by Blume, Freeman, and Watson,[22] and then comparing the magnetic intensities with the nuclear intensities. The results obtained for the three materials studied here are given in Table I. The superconducting transition temperatures are taken from the resistivity and susceptibility data,[9,17] and the magnetic ordering temperatures from the magnetic order parameters measured in the neutron scattering experiments. The values for the magnetic moments calculated from the neutron data are smaller than the free-ion values. This is presumably due to the importance of crystalline field effects. The values obtained by neutrons for the Tb^{3+} and Dy^{3+} ions are also larger than obtained by magnetization measurements.[17]

The amount of information obtainable from a powder pattern concerning the details of the spin direction is limited, particularly for high-symmetry crystals.[23] For a tetragonal magnetic structure, only the angle ϕ can be determined. However, these Chevrel phase materials have a small trigonal distortion which reduces the symmetry and therefore some of the magnetic-peak groups will be split. In particular, we have measured, with high-resolution scans, the $\{10\frac{3}{2}\}$ peak for the $DyMo_6S_8$ and $TbMo_6S_8$. This scan for the $TbMo_6S_8$ is shown in Fig. 4. The line through the points is the result of a least-squares fit of two Gaussian peaks, from which the intensity ratio in the peaks can be determined.

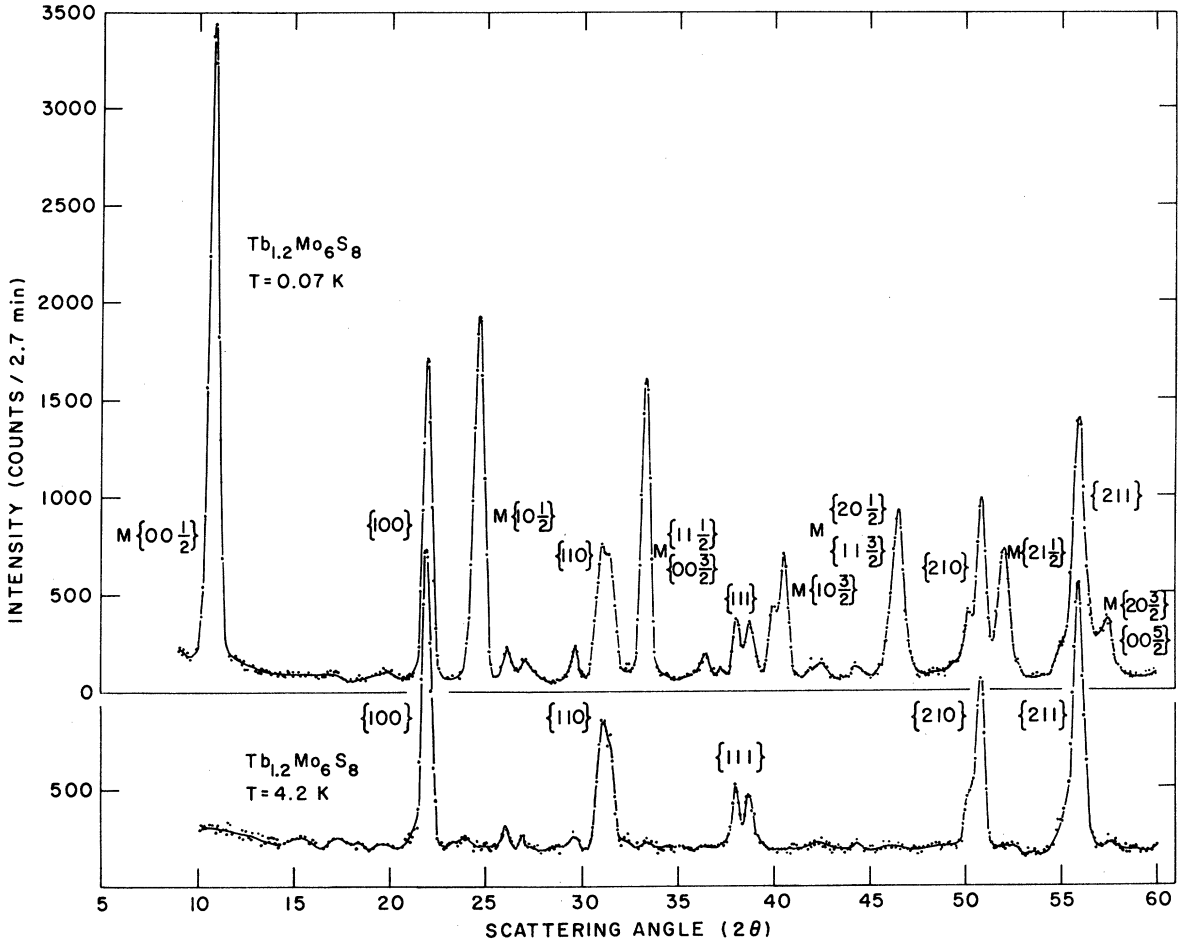

FIG. 3. Powder neutron-diffraction data for $TbMo_6S_8$ above ($T=4.2$ K) and below ($T=0.07$ K) the antiferromagnetic ordering transition at $T_M=1.05$ K.

It was noted for the $DyMo_6S_8$ that the angle $\phi=55°$ was essentially the same as the angle which the [111] direction makes with $\vec{q}_m$. The spin direction was then assumed to lie either along [111] or [11$\bar{1}$] and the appropriate magnetic interaction vectors were calculated. The measured intensity ratio was

$$I(10\tfrac{\bar{3}}{2})/I(10\tfrac{3}{2})=2.55\pm0.4\ .$$

TABLE I. Superconducting (T_c) and magnetic ordering (T_M) temperatures, and the magnetic moment of the rare-earth ions calculated from the neutron-diffraction data.

	T_c (K)	T_M (K)	μ (μ_B)
$TbMo_6S_8$	2.05	1.05	8.3 ±0.2
$DyMo_6S_8$	2.05	0.4	8.8 ±0.2
$ErMo_6S_8$	2.2	0.2	3.5 ±0.3

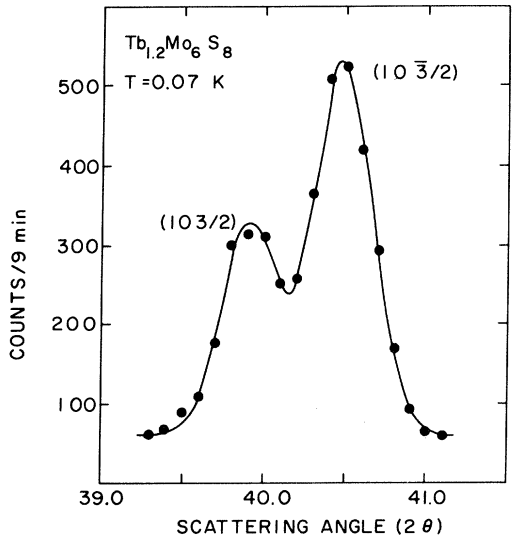

FIG. 4. High-resolution scans through the $\{10\frac{3}{2}\}$ peak in $TbMo_6S_8$ showing the splitting of the peak due to the small rhombohedral distortion. The solid line is a least-squares fit of two Gaussian peaks.

The calculated magnetic intensity ratios were

$$\frac{I(10\bar{\frac{3}{2}})}{I(10\frac{3}{2})} = \begin{cases} 2.71 \text{ with magnetic moment along } [111] \\ 0.37 \text{ with magnetic moment along } [11\bar{1}] \\ 1.0 \text{ with magnetic moment along } [1\bar{1}1] \end{cases}.$$

This comparison allowed us to conclude that the moment must lie along the [111] axis.

The situation for the $TbMo_6S_8$ was somewhat different since the angle $\phi \approx 60°$ does not lie along any symmetry direction. However, the measured intensity ratio

$$I(10\bar{\frac{3}{2}})/I(10\frac{3}{2}) = 1.97 \pm 0.1$$

can again be used to determine the direction of the moment. The intensity ratio can be calculated for an arbitrary direction of the moment with the constraint that $\phi = 60°$. A unit vector for the moment can then be defined as $\bar{S} = (\frac{1}{2}\sqrt{3}\cos\beta, \frac{1}{2}\sqrt{3}\sin\beta, \frac{1}{2})$, where β is the angle in the (001) plane measured relative to the [100] direction. A calculated ratio of 1.97 is acheived for $\beta = 10°$. Thus the moment direction is $[hkl] = [0.85\ 0.15\ 0.5]$. We can make no statement concerning the $ErMo_6S_8$ other than $\phi \approx 45°$, since the $\{10\frac{3}{2}\}$ peak data were not good enough to allow a reasonable estimate of the intensity ratio. The magnetic ordering temperatures shown in Table I have been arrived at by examination of the temperature dependence of the $\{00\frac{1}{2}\}$ peak intensity. We have calculated the effective magnetization μ_{eff} for each temperature and plotted the results in Fig. 5. There is no observable hysteresis in the data on warming and cooling. The data are for zero applied magnetic field, except for the $ErMo_6S_8$ for which a remanent field of ~ 250 Oe was present.

The inset of Fig. 5 shows upper-critical-field data of Ishikawa and Fischer.[9] A comparison of the temperatures of the H_{c2} anomalies with the onset of magnetic order for the $TbMo_6S_8$ and $DyMo_6S_8$ samples clearly demonstrates an interaction between the magnetic order and the superconductivity. The anomaly in H_{c2} for the $DyMo_6S_8$ saturates when the staggered magnetization reaches saturation. This suggests that the reduction in H_{c2} in the magnetic state is produced by an additional, nearly-field-independent, pair-breaking parameter which varies as the magnetic order parameter. The $TbMo_6S_8$ displays somewhat different behavior in that H_{c2} increases again as the temperature is lowered well below T_M.

B. Applied magnetic fields

In order to investigate the question of the magnetic structure in an applied magnetic field, the dilution refrigerator was inserted into a superconducting magnet. The results for $TbMo_6S_8$ at $T = 0.06$ K at low fields ($H < 6$ kOe) are shown in Fig. 6 and for higher fields in Fig. 7. The peak intensity of the antiferromagnetic $\{10\frac{1}{2}\}$ peak is seen to monotonically

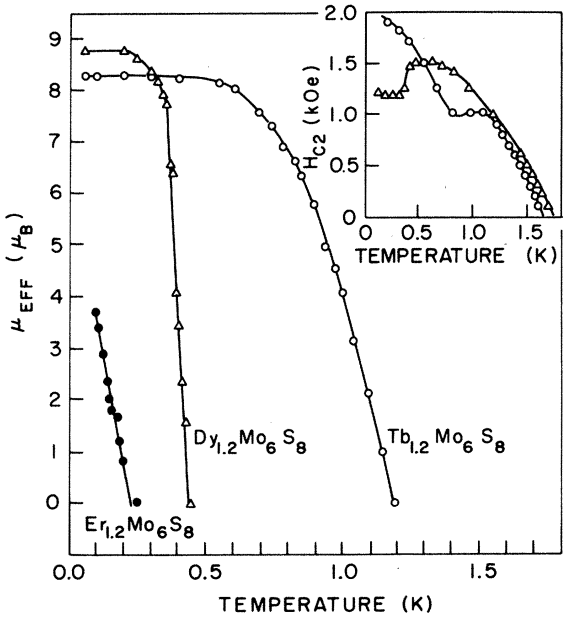

FIG. 5. Temperature dependence of the magnetization for $(R)Mo_6S_8$ (R = Tb, Dy, Er) as determined by neutron diffraction. The inset shows H_{c2} for the Tb and Dy compounds as determined by Ishikawa and Fischer, Ref. 9.

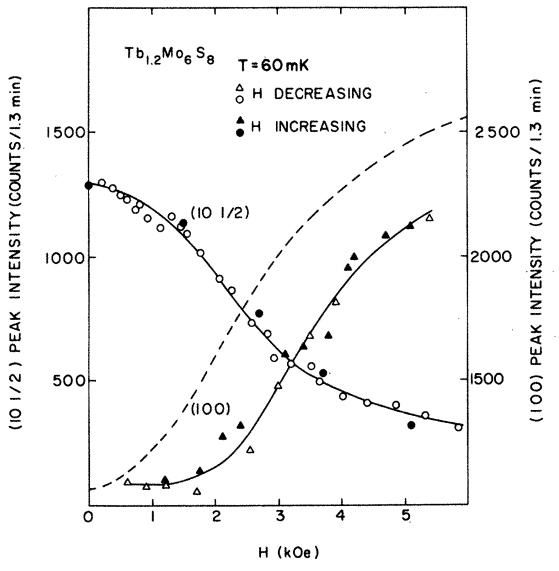

FIG. 6. Antiferromagnetic $\{10\frac{1}{2}\}$ and ferromagnetic $\{100\}$ neutron scattering peak intensities for $TbMo_6S_8$ at $T = 0.06$ K as a function of the applied magnetic field. The solid lines are guides to the eye. The dashed line is the calculated ferromagnetic intensity based on the measured $\{10\frac{1}{2}\}$ intensity.

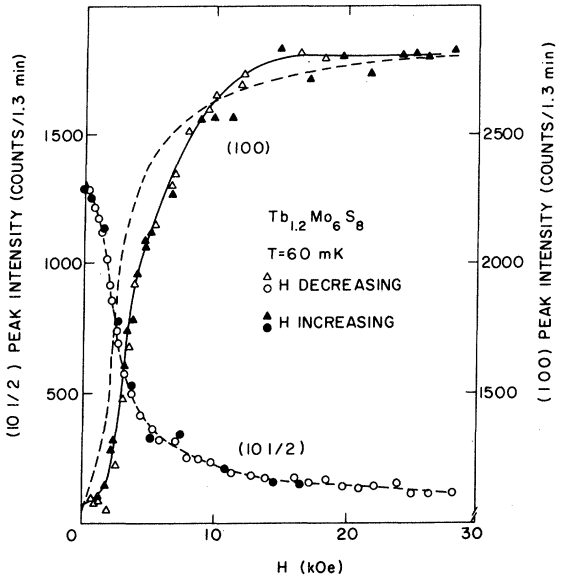

FIG. 7. Same data as Fig. 6 but showing the intensities for magnetic fields up to 28 kOe.

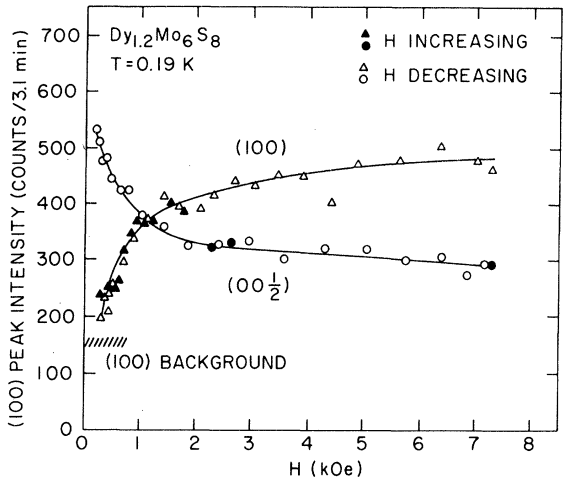

FIG. 8. Antiferromagnetic $\{00\frac{1}{2}\}$ and ferromagnetic {100} neutron scattering peak intensities for $DyMo_6S_8$ at $T=0.19$ K as a function of the applied magnetic field. The solid curve through the $\{00\frac{1}{2}\}$ data is a guide to the eye. The ferromagnetic intensities calculated from the $\{00\frac{1}{2}\}$ data are shown by the solid line through the {100} data.

decrease as the field increases. The intensity is proportional to the square of the staggered magnetization. In these measurements, the positions of the peaks were checked to verify that they did not shift with field. The intensity continued to slowly decrease even at $H=30$ kOe. That behavior is similar to the observation that the magnetization of $TbMo_6S_8$ could not be saturated in fields as high as 18.5 kOe.[17] The intensity of the {100} peak in Figs. 6 and 7 consists of a field-independent nuclear scattering background plus the magnetic scattering due to the induced ferromagnetic ordering of the Tb moments in the applied field. Very little ferromagnetic intensity develops for $H < H_{c2}=1.9$ kOe. The ferromagnetic peaks were, like the antiferromagnetic peaks, resolution limited. Thus the induced ferromagnetism is also associated with a correlation length greater than 300 Å.

In Figs. 6 and 7, a solid line has been drawn through the data for the $\{10\frac{1}{2}\}$ peak intensity. If we assume that it represents the square of the magnetization, M^2, and that the ferromagnetic intensity is proportional to $(1-M)^2$, then we can calculate the expected {100} peak intensity. The results are shown by the dashed lines. This simple model overestimates the ferromagnetic component at low fields, and underestimates it at high fields.

The magnetization calculated from the square root of the measured magnetic contribution to the {100} peak has been normalized to the data of Ishikawa and Muller[17] at 4 kOe and plotted with their data in Fig. 2. The neutron data are in good agreement with the magnetization measurements and confirm that ferromagnetic order develops for fields greater than about 1.6 kOe.

A similar set of data on $DyMo_6S_8$ is shown in Fig. 8 at $T=0.19$ K. The striking feature of these data is the rapid increase of the ferromagnetic component of the {100} peak at low fields. Below $H_{c2}\sim 1.2$ kOe both long-range ferromagnetic and antiferromagnetic order occur with the sample in the superconducting state. In this sample a calculation of the {100} ferromagnetic contribution based on the antiferromagnetic $\{00\frac{1}{2}\}$ intensity is in excellent agreement with the data, as shown in Fig. 8 by the solid lines. The magnetization calculated from the {100} peak intensity is also in agreement with the magnetization data of Ishikawa and Muller, shown in Fig. 2. At an applied field near but less than H_{c2}, the ferromagnetic magnetization is already about 80% of the saturation value. The neutron data do not give a detailed microscopic picture of where the ferromagnetic order is developing. It cannot necessarily be concluded that the induced ferromagnetism is coexisting with the superconductivity in the same manner as the antiferromagnetism. The ferromagnetism may occur in domains or along flux lines,[24] for example. A study of the {100} linewidth at a field of 600 Oe showed it to be resolution limited, so the ferromagnetic order of the Dy moments has a correlation range greater than 300 Å.

C. $ErMo_6S_8$

The $ErMo_6S_8$ sample which we studied can be characterized as an incipient antiferromagnet. It was

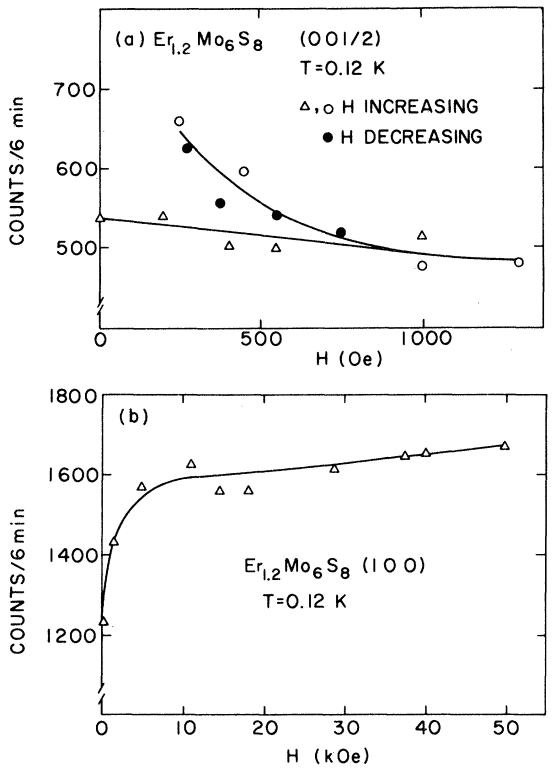

FIG. 9. (a) Magnetic field dependence of the $\{00\frac{1}{2}\}$ peak intensity in $ErMo_6S_8$. The open triangles are for increasing magnetic field following the initial cooldown of the sample in zero applied field. The magnetic field was then increased to $H=20$ kOe and decreased to 250 Oe. The solid circles and open circles, respectively, show the reversible development of antiferromagnetic intensity as the field was decreased and increased. (b) The peak intensity of the {100} reflection as a function of increasing magnetic field showing the development of ferromagnetic order.

initially cooled in zero external applied field to $T=0.11$ K with no measurable magnetic order developing. The magnetic field was then increased to $H=20$ kOe, the low-field intensities at an angle corresponding to the position of a $\{00\frac{1}{2}\}$ peak being plotted in Fig. 9. When the magnetic field was subsequently lowered to its minimum value of 250 Oe, the sample showed antiferromagnetic order developing. In fact, the antiferromagnetism then was similar in character to the $DyMo_6S_8$ and $TbMo_6S_8$ in the sense that it was the same magnetic structure and was reversible with both temperature and field. The temperature dependence of the magnetic moment is shown in Fig. 5 and the magnetic field dependence of the $\{00\frac{1}{2}\}$ peak intensity is shown in Fig. 9. The field could not be decreased below 250 Oe after the magnet was turned on during the experiment due to the remanent field of the magnet. The powder pattern in the magnetic state was consistent with the structure being (001) planes of spins alternating in spin direction. Only the angle ϕ, given above, could be determined. A good measurement of the $\{10\frac{3}{2}\}$ peak could not be made. The magnetic moment of the Er^{3+} ions was calculated to be $(3.5\pm0.3)\mu_B$. This value is calculated both from the low-temperature antiferromagnetic-peak data (which may not be completely saturated since the order parameter has not completely saturated at $T=0.11$ K) and from the high-field ferromagnetic {100} contribution. As seen in Fig. 9 this is not completely saturated even at 50 kOe.

It is not known why we observed the incipient behavior in this sample. It is perhaps due to strains in the crystals which are overcome by the application of the high fields. We also do not know what would happen if the field were really reduced to zero at low temperatures.

ACKNOWLEDGMENTS

We are grateful to D. E. Cox and J. W. Lynn for helpful discussions concerning the analysis of the data. Work at Brookhaven was supported by the Division of Basic Energy Sciences, U.S. Department of Energy, under Contract No. DE-AC02-76-CH00016.

[1]For a recent reference and guide to earlier literature, see J. W. Lynn, D. E. Moncton, L. Passell, and W. Thomlinson, Phys. Rev. B 21, 70 (1980).

[2]A. A. Abrikosov and L. P. Gorkov, Zh. Eksp. Teor. Fiz. 39, 1781 (1960) [Sov. Phys. JETP 12, 1243 (1961)].

[3]Ø. Fischer, A. Treyvaud, R. Chevrel, and M. Sergent, Solid State Commun. 17, 721 (1975).

[4]R. N. Shelton, R. W. McCallum, and A. Adrain, Phys. Lett. 56A, 213 (1976).

[5]B. T. Matthias, E. Corenzwit, J. M. Vandenberg, and H. E. Bartz, Prog. Nat. Acad. Sci. USA 74, 1334 (1977).

[6]W. A. Fertig, D. C. Johnston, L. E. DeLong, R. W. McCallum, M. B. Maple, and B. T. Matthias, Phys. Rev. Lett. 38, 987 (1977).

[7]M. Ishikawa and Ø. Fischer, Solid State Commun. 23, 37 (1977).

[8]R. W. McCallum, D. C. Johnston, R. N. Shelton, W. A. Fertig, and M. B. Maple, Solid State Commun. 24, 501 (1977).

[9]M. Ishikawa and Ø. Fischer, Solid State Commun. 24, 747 (1977).

[10]D. E. Moncton, D. B. McWhan, J. Eckert, G. Shirane, and

W. Thomlinson, Phys. Rev. Lett. 39, 1164 (1977).
[11]J. W. Lynn, D. E. Moncton, W. Thomlinson, G. Shirane, and R. N. Shelton, Solid State Commun. 26, 493 (1978).
[12]J. W. Lynn, G. Shirane, W. Thomlinson, and R. N. Shelton (unpublished).
[13]D. E. Moncton, G. Shirane, and W. Thomlinson, J. Magn. Magn. Mater. 14, 172 (1979).
[14]D. E. Moncton, D. B. McWhan, P. H. Schmidt, G. Shirane, W. Thomlinson, M. B. Maple, H. B. MacKay, L. D. Woolf, Z. Fisk, and D. C. Johnston, Phys. Rev. Lett. 45, 2060 (1980).
[15]M. B. Maple, J. Phys. Suppl. C 6, 1374 (1978).
[16]M. Ishikawa, Ø. Fischer, and J. Muller, J. Phys. Suppl. C 6, 1379 (1978).
[17]M. Ishikawa and J. Muller, Solid State Commun. 27, 761 (1978).
[18]D. E. Moncton, G. Shirane, W. Thomlinson, M. Ishikawa, and Ø. Fischer, Phys. Rev. Lett. 41, 1133 (1978).
[19]W. Thomlinson, G. Shirane, D. E. Moncton, M. Ishikawa, and Ø. Fischer, J. Appl. Phys. 50, 1981 (1979).
[20]C. F. Majkrzak, G. Shirane, W. Thomlinson, M. Ishikawa, Ø. Fischer, and D. E. Moncton, Solid State Commun. 31, 773 (1979).
[21]K. Yvon, in *Current Topics in Materials Science,* edited by E. Kaldis (North-Holland, New York, 1978), Chap. 2.
[22]M. Blume, A. J. Freeman, and R. E. Watson, J. Chem. Phys. 37, 1345 (1962).
[23]G. Shirane, Acta Crystallogr. 12, 282 (1959).
[24]T. Krzyston, J. Magn. Magn. Mater. 15, 1572 (1980).